

Study of the  $e^+e^- \rightarrow D^{(*)}\bar{D}^{(*)}$  cross section in the center of mass energy range near  $D^{(*)}\bar{D}^{(*)}$  threshold with initial state radiation

K. Abe,<sup>9</sup> K. Abe,<sup>49</sup> I. Adachi,<sup>9</sup> H. Aihara,<sup>51</sup> D. Anipko,<sup>1</sup> K. Aoki,<sup>25</sup> T. Arakawa,<sup>32</sup>  
 K. Arinstein,<sup>1</sup> Y. Asano,<sup>56</sup> T. Aso,<sup>55</sup> V. Aulchenko,<sup>1</sup> T. Aushev,<sup>21</sup> T. Aziz,<sup>47</sup> S. Bahinipati,<sup>4</sup>  
 A. M. Bakich,<sup>46</sup> V. Balagura,<sup>15</sup> Y. Ban,<sup>37</sup> S. Banerjee,<sup>47</sup> E. Barberio,<sup>24</sup> M. Barbero,<sup>8</sup>  
 A. Bay,<sup>21</sup> I. Bedny,<sup>1</sup> K. Belous,<sup>14</sup> U. Bitenc,<sup>16</sup> I. Bizjak,<sup>16</sup> S. Blyth,<sup>27</sup> A. Bondar,<sup>1</sup>  
 A. Bozek,<sup>30</sup> M. Bracko,<sup>23,16</sup> J. Brodzicka,<sup>9,30</sup> T. E. Browder,<sup>8</sup> M.-C. Chang,<sup>50</sup> P. Chang,<sup>29</sup>  
 Y. Chao,<sup>29</sup> A. Chen,<sup>27</sup> K.-F. Chen,<sup>29</sup> W. T. Chen,<sup>27</sup> B. G. Cheon,<sup>3</sup> R. Chistov,<sup>15</sup>  
 J. H. Choi,<sup>18</sup> S.-K. Choi,<sup>7</sup> Y. Choi,<sup>45</sup> Y. K. Choi,<sup>45</sup> A. Chuvikov,<sup>39</sup> S. Cole,<sup>46</sup> J. Dalseno,<sup>24</sup>  
 M. Danilov,<sup>15</sup> M. Dash,<sup>57</sup> R. Dowd,<sup>24</sup> J. Dragic,<sup>9</sup> A. Dnutskey,<sup>4</sup> S. Eideman,<sup>1</sup> Y. Enari,<sup>25</sup>  
 D. Epifanov,<sup>1</sup> S. Fratina,<sup>16</sup> H. Fujii,<sup>9</sup> M. Fujikawa,<sup>26</sup> N. Gabyshev,<sup>1</sup> A. Gamash,<sup>39</sup>  
 T. Gerstner,<sup>9</sup> A. Go,<sup>27</sup> G. Gokhroo,<sup>47</sup> P. Goldenzweig,<sup>4</sup> B. Golob,<sup>22,16</sup> A. Gorisek,<sup>16</sup>  
 M. Grosse Perdekamp,<sup>11,40</sup> H. Guler,<sup>8</sup> H. Ha,<sup>18</sup> J. Haba,<sup>9</sup> K. Hara,<sup>25</sup> T. Hara,<sup>35</sup>  
 Y. Hasegawa,<sup>44</sup> N. C. Hastings,<sup>51</sup> K. Hayasaka,<sup>25</sup> H. Hayashii,<sup>26</sup> M. Hazumi,<sup>9</sup>  
 D. Heeman,<sup>35</sup> T. Higuchi,<sup>9</sup> L. Hinz,<sup>21</sup> T. Hokuue,<sup>25</sup> Y. Hoshi,<sup>49</sup> K. Hoshina,<sup>54</sup> S. Hou,<sup>27</sup>  
 W.-S. Hou,<sup>29</sup> Y. B. Hsiung,<sup>29</sup> Y. Igarashi,<sup>9</sup> T. Iijima,<sup>25</sup> K. Ikado,<sup>25</sup> A. Imoto,<sup>26</sup> K. Inami,<sup>25</sup>  
 A. Ishikawa,<sup>51</sup> H. Ishino,<sup>52</sup> K. Itoh,<sup>51</sup> R. Itoh,<sup>9</sup> M. Iwabuchi,<sup>6</sup> M. Iwasaki,<sup>51</sup> Y. Iwasaki,<sup>9</sup>  
 C. Jacoby,<sup>21</sup> M. Jones,<sup>8</sup> H. Kakuno,<sup>51</sup> J. H. Kang,<sup>58</sup> J. S. Kang,<sup>18</sup> P. Kapusta,<sup>30</sup>  
 S. U. Katakawa,<sup>26</sup> N. Katayama,<sup>9</sup> H. Kawai,<sup>2</sup> T. Kawasaki,<sup>32</sup> H. R. Khan,<sup>52</sup> A. Kibayashi,<sup>52</sup>  
 H. Kichimi,<sup>9</sup> N. Kikuchi,<sup>50</sup> H. J. Kim,<sup>20</sup> H. O. Kim,<sup>45</sup> J. H. Kim,<sup>45</sup> S. K. Kim,<sup>43</sup>  
 T. H. Kim,<sup>58</sup> Y. J. Kim,<sup>6</sup> K. Kinoshita,<sup>4</sup> N. Kishimoto,<sup>25</sup> S. Korpar,<sup>23,16</sup> Y. Kozakai,<sup>25</sup>  
 P. Krizan,<sup>22,16</sup> P. Krokovny,<sup>9</sup> T. Kubota,<sup>25</sup> R. Kulasiri,<sup>4</sup> R. Kumar,<sup>36</sup> C. C. Kuo,<sup>27</sup>  
 E. Kurihara,<sup>2</sup> A. Kusaka,<sup>51</sup> A. Kuzmin,<sup>1</sup> Y.-J. Kwon,<sup>58</sup> J. S. Lange,<sup>5</sup> G. Leder,<sup>13</sup> J. Lee,<sup>43</sup>  
 S. E. Lee,<sup>43</sup> Y.-J. Lee,<sup>29</sup> T. Lesiak,<sup>30</sup> J. Li,<sup>8</sup> A. Limosani,<sup>9</sup> C. Y. Lin,<sup>29</sup> S.-W. Lin,<sup>29</sup>  
 Y. Liu,<sup>6</sup> D. Liventsev,<sup>15</sup> J. Madnaughton,<sup>13</sup> G. Majumder,<sup>47</sup> F. Mandl,<sup>13</sup> D. Marlow,<sup>39</sup>  
 T. Matsumoto,<sup>53</sup> A. Matyjka,<sup>30</sup> S. Mönig,<sup>46</sup> T. Medvedeva,<sup>15</sup> Y. Mikami,<sup>50</sup> W. Mitaro,<sup>13</sup>  
 K. Miyabayashi,<sup>26</sup> H. Miyake,<sup>35</sup> H. Miyata,<sup>32</sup> Y. Miyazaki,<sup>25</sup> R. Mizuk,<sup>15</sup> D. Mohapatra,<sup>57</sup>  
 G. R. Molloney,<sup>24</sup> T. Mori,<sup>52</sup> J. Mueller,<sup>38</sup> A. Murakami,<sup>41</sup> T. Nagamine,<sup>50</sup> Y. Nagasaka,<sup>10</sup>  
 T. Nakagawa,<sup>53</sup> Y. Nakahama,<sup>51</sup> I. Nakamura,<sup>9</sup> E. Nakano,<sup>34</sup> M. Nakao,<sup>9</sup> H. Nakazawa,<sup>9</sup>  
 Z. Natkaniec,<sup>30</sup> K. Neichi,<sup>49</sup> S. Nishida,<sup>9</sup> K. Nishimura,<sup>8</sup> O. Nitoh,<sup>54</sup> S. Noguchi,<sup>26</sup>  
 T. Nozaki,<sup>9</sup> A. Ogawa,<sup>40</sup> S. Ogawa,<sup>48</sup> T. Ohshima,<sup>25</sup> T. Okabe,<sup>25</sup> S. Okuno,<sup>17</sup> S. L. Olsen,<sup>8</sup>  
 S. Ono,<sup>52</sup> W. Ostrowicz,<sup>30</sup> H. Ozaki,<sup>9</sup> P. Pakhlov,<sup>15</sup> G. Pakhlova,<sup>15</sup> H. Palka,<sup>30</sup>  
 C. W. Park,<sup>45</sup> H. Park,<sup>20</sup> K. S. Park,<sup>45</sup> N. Parslow,<sup>46</sup> L. S. Peak,<sup>46</sup> M. Pemicka,<sup>13</sup>  
 R. Pestotnik,<sup>16</sup> M. Peters,<sup>8</sup> L. E. Piihonen,<sup>57</sup> A. Poluektov,<sup>1</sup> F. J. Ronga,<sup>9</sup> N. Root,<sup>1</sup>  
 J. Rorie,<sup>8</sup> M. Rozanska,<sup>30</sup> H. Sahoo,<sup>8</sup> S. Saitoh,<sup>9</sup> Y. Sakai,<sup>9</sup> H. Sakamoto,<sup>19</sup> H. Sakaue,<sup>34</sup>  
 T. R. Sarangi,<sup>6</sup> N. Sato,<sup>25</sup> N. Satoyama,<sup>44</sup> K. Sayeed,<sup>4</sup> T. Schietinger,<sup>21</sup> O. Schneider,<sup>21</sup>  
 P. Schonmeyer,<sup>50</sup> J. Schumann,<sup>28</sup> C. Schwanda,<sup>13</sup> A. J. Schwartz,<sup>4</sup> R. Seidl,<sup>11,40</sup> T. Seki,<sup>53</sup>  
 K. Senyo,<sup>25</sup> M. E. Sevier,<sup>24</sup> M. Shapkin,<sup>14</sup> Y.-T. Shen,<sup>29</sup> H. Shibuya,<sup>48</sup> B. Schwartz,<sup>1</sup>  
 V. Sidorov,<sup>1</sup> J. B. Singh,<sup>36</sup> A. Sokolov,<sup>14</sup> A. Somov,<sup>4</sup> N. Soni,<sup>36</sup> R. Stamen,<sup>9</sup> S. Stanic,<sup>33</sup>  
 M. Staric,<sup>16</sup> H. Stoeck,<sup>46</sup> A. Sugiyama,<sup>41</sup> K. Sumisawa,<sup>9</sup> T. Sumiyoshi,<sup>53</sup> S. Suzuki,<sup>41</sup>  
 S. Y. Suzuki,<sup>9</sup> O. Tajima,<sup>9</sup> N. Takada,<sup>44</sup> F. Takasaki,<sup>9</sup> K. Tamai,<sup>9</sup> N. Tamura,<sup>32</sup>

K. Tanabe,<sup>51</sup> M. Tanaka,<sup>9</sup> G. N. Taylor,<sup>24</sup> Y. Teramoto,<sup>34</sup> X. C. Tian,<sup>37</sup> I. Tikhomirov,<sup>15</sup>  
 K. Trabelsi,<sup>9</sup> Y. T. Tsai,<sup>29</sup> Y. F. Tseng,<sup>24</sup> T. Tsuboyama,<sup>9</sup> T. Tsubokawa,<sup>9</sup> K. Uchida,<sup>8</sup>  
 Y. Uchida,<sup>6</sup> S. Uehara,<sup>9</sup> T. Uglav,<sup>15</sup> K. Ueno,<sup>29</sup> Y. Unno,<sup>9</sup> S. Uno,<sup>9</sup> P. Urquijo,<sup>24</sup>  
 Y. Ushiroda,<sup>9</sup> Y. Usov,<sup>1</sup> G. Vamer,<sup>8</sup> K. E. Varvell,<sup>46</sup> S. Villa,<sup>21</sup> C. C. Wang,<sup>29</sup>  
 C. H. Wang,<sup>28</sup> M. Z. Wang,<sup>29</sup> M. Watanabe,<sup>32</sup> Y. Watanabe,<sup>52</sup> J. Wicht,<sup>21</sup> L. Widhalm,<sup>13</sup>  
 J. Wiederczynski,<sup>30</sup> E. Won,<sup>18</sup> C. H. Wu,<sup>29</sup> Q. L. Xie,<sup>12</sup> B. D. Yabsley,<sup>46</sup> A. Yamaguchi,<sup>50</sup>  
 H. Yamamoto,<sup>50</sup> S. Yamamoto,<sup>53</sup> Y. Yamashita,<sup>31</sup> M. Yamachi,<sup>9</sup> Heyoung Yang,<sup>43</sup>  
 S. Yoshino,<sup>25</sup> Y. Yuan,<sup>12</sup> Y. Yusa,<sup>57</sup> S. L. Zang,<sup>12</sup> C. C. Zhang,<sup>12</sup> J. Zhang,<sup>9</sup>  
 L. M. Zhang,<sup>42</sup> Z. P. Zhang,<sup>42</sup> V. Zhilich,<sup>1</sup> T. Ziegler,<sup>39</sup> A. Zupanc,<sup>16</sup> and D. Zurcher<sup>21</sup>

(The Belle Collaboration)

<sup>1</sup>Budker Institute of Nuclear Physics, Novosibirsk

<sup>2</sup>Chiba University, Chiba

<sup>3</sup>Chonnam National University, Kwangju

<sup>4</sup>University of Cincinnati, Cincinnati, Ohio 45221

<sup>5</sup>University of Frankfurt, Frankfurt

<sup>6</sup>The Graduate University for Advanced Studies, Hayama

<sup>7</sup>Gyeongsang National University, Chinju

<sup>8</sup>University of Hawaii, Honolulu, Hawaii 96822

<sup>9</sup>High Energy Accelerator Research Organization (KEK), Tsukuba

<sup>10</sup>Hiroshima Institute of Technology, Hiroshima

<sup>11</sup>University of Illinois at Urbana-Champaign, Urbana, Illinois 61801

<sup>12</sup>Institute of High Energy Physics,

Chinese Academy of Sciences, Beijing

<sup>13</sup>Institute of High Energy Physics, Vienna

<sup>14</sup>Institute of High Energy Physics, Protvino

<sup>15</sup>Institute for Theoretical and Experimental Physics, Moscow

<sup>16</sup>J. Stefan Institute, Ljubljana

<sup>17</sup>Kanagawa University, Yokohama

<sup>18</sup>Korea University, Seoul

<sup>19</sup>Kyoto University, Kyoto

<sup>20</sup>Kyungpook National University, Taegu

<sup>21</sup>Swiss Federal Institute of Technology of Lausanne, EPFL, Lausanne

<sup>22</sup>University of Ljubljana, Ljubljana

<sup>23</sup>University of Maribor, Maribor

<sup>24</sup>University of Melbourne, Victoria

<sup>25</sup>Nagoya University, Nagoya

<sup>26</sup>Nara Women's University, Nara

<sup>27</sup>National Central University, Chung-li

<sup>28</sup>National United University, Miao Li

<sup>29</sup>Department of Physics, National Taiwan University, Taipei

<sup>30</sup>H. Niewodniczanski Institute of Nuclear Physics, Krakow

<sup>31</sup>Nippon Dental University, Niigata

<sup>32</sup>Niigata University, Niigata

<sup>33</sup>University of Nova Gorica, Nova Gorica

<sup>34</sup>Osaka City University, Osaka

<sup>35</sup>Osaka University, Osaka

- <sup>36</sup>Panjab University, Chandigarh  
<sup>37</sup>Peking University, Beijing  
<sup>38</sup>University of Pittsburgh, Pittsburgh, Pennsylvania 15260  
<sup>39</sup>Princeton University, Princeton, New Jersey 08544  
<sup>40</sup>RIKEN BNL Research Center, Upton, New York 11973  
<sup>41</sup>Saga University, Saga  
<sup>42</sup>University of Science and Technology of China, Hefei  
<sup>43</sup>Seoul National University, Seoul  
<sup>44</sup>Shinshu University, Nagano  
<sup>45</sup>Sungkyunkwan University, Suwon  
<sup>46</sup>University of Sydney, Sydney NSW  
<sup>47</sup>Tata Institute of Fundamental Research, Bombay  
<sup>48</sup>Toho University, Funabashi  
<sup>49</sup>Tohoku Gakuin University, Tagajō  
<sup>50</sup>Tohoku University, Sendai  
<sup>51</sup>Department of Physics, University of Tokyo, Tokyo  
<sup>52</sup>Tokyo Institute of Technology, Tokyo  
<sup>53</sup>Tokyo Metropolitan University, Tokyo  
<sup>54</sup>Tokyo University of Agriculture and Technology, Tokyo  
<sup>55</sup>Toyama National College of Maritime Technology, Toyama  
<sup>56</sup>University of Tsukuba, Tsukuba  
<sup>57</sup>Virginia Polytechnic Institute and State University, Blacksburg, Virginia 24061  
<sup>58</sup>Yonsei University, Seoul

### Abstract

We report measurements of the exclusive  $e^+e^- \rightarrow D^{(*)} \bar{D}^{(*)}$  cross section as a function of center-of-mass energy near the  $D^{(*)} \bar{D}^{(*)}$  threshold with initial state radiation. A partial reconstruction technique involving full reconstruction of one  $D^{(*)}$  and reconstruction of the slow pion from the other  $D^{(*)}$  is used to increase the efficiency and to suppress background. The analysis is based on a data sample collected with the Belle detector at the  $\Upsilon(4S)$  resonance and nearby continuum with an integrated luminosity of  $547.8 \text{ fb}^{-1}$  at the KEKB asymmetric energy  $e^+e^-$  collider.

PACS numbers:

## INTRODUCTION

The  $e^+e^-$  hadronic cross section for all values of  $\sqrt{s}$  is essential input to the calculation of vacuum polarization and, therefore, has an important influence on the determination of many parameters of the Standard Model. The region of  $\sqrt{s}$  below open-charm threshold has been measured by a number of experiments. Above the open-charm threshold, BES [1] and the Crystal Ball [2] have measured the inclusive hadronic cross-section with good precision over the region  $3.7 \text{ GeV} < \sqrt{s} < 5 \text{ GeV}$ . However, the cross sections for exclusive open-charm final states are not as well known. CLEO-c recently reported precision measurements of exclusive cross sections for  $D\bar{D}^*$ ,  $D\bar{D}^0$ ,  $D\bar{D}^+$ ,  $J^P = 0^-$  and  $J^P = 1^-$   $K^+K^-$  final states, as well as the inclusive  $e^+e^-$  hadronic cross sections at twelve energy points between 3.970 to 4.260 GeV [3, 4]. BES reported a measurement of the total charm production cross section at  $\sqrt{s} = 4.04 \text{ GeV}$ .

Exclusive cross sections for specific charm ed-particle final states are of particular interest because they provide information on the spectrum of  $J^{PC} = 1^-$  charm onium states above the open-charm threshold, which are not well understood. Most of the known states in this energy region decay to open charm pairs. However, the recently discovered charm onium-like  $Y(4260)$  state has only been seen in  $J^P = 1^-$  final states [4, 5]. In fact, the mass,  $4.260 \text{ GeV} = c^2$ , is surprisingly close to a local minimum of the total hadronic cross section.

In this paper we report on a study of exclusive cross sections for  $e^+e^- \rightarrow D^+D^-$  and  $e^+e^- \rightarrow D^+D^0$  [6] using initial state radiation (ISR).

## METHOD

To measure the  $e^+e^-$  hadronic cross section at  $\sqrt{s}$  smaller than the initial  $e^+e^-$  CM energy ( $E_{CM}$ ) at B-factories, initial state radiation (radiative return) can be used. Radiative return offers the unique possibility of measuring cross sections over a continuum of energies. The high luminosity of the B-factories compensates for the suppression associated with the emission of a hard photon. The method was pioneered by BaBar for light hadron final states [7]. Here we report results from an application of an adaptation of this method for cross section measurements for  $e^+e^-$  annihilation into exclusive  $D^+D^-$  and  $D^+D^0$  final states.

The selection of  $e^+e^- \rightarrow D^{(\prime)+}D^-$  ISR signal events using full reconstruction of both the  $D^{(\prime)+}$  &  $D^-$  mesons, plus the ISR photon, suffers from low efficiency due to the low  $D^{(\prime)+}$  reconstruction efficiencies, small branching fractions and the low geometrical acceptance for the ISR, which tends to be emitted along the beam line. A selection that uses fully reconstructed  $D^{(\prime)+}$  and  $D^-$  while not requiring the ISR to be detected does not significantly improve the final efficiency: the kinematic region where the ISR is outside of the detector acceptance corresponds to a tiny  $D^-$  reconstruction efficiency because of the small  $p_T$  of the slow pions from  $D^-$  decays in this case.

Here we use a method that achieves higher efficiency by requiring full reconstruction of only one of  $D^{(\prime)+}$  [6] mesons, the ISR, and the slow pion from the other  $D^-$ . In this case the the spectrum of masses recoiling against the  $D^{(\prime)+}$  ISR system :

$$M_{\text{recoil}}(D^{(\prime)+}_{\text{ISR}}) = \frac{q}{(E_{\text{CM}} - E(D^{(\prime)+}_{\text{ISR}}))^2 - p^2(D^{(\prime)+}_{\text{ISR}})}; \quad (1)$$

peaks at the  $D^-$  mass. Here  $E(D^{(\prime)+}_{\text{ISR}})$  and  $p(D^{(\prime)+}_{\text{ISR}})$  are the center of mass (CM)

energy and momentum of the  $D^{(\pm)+}_{ISR}$  combination, respectively. We illustrate the method

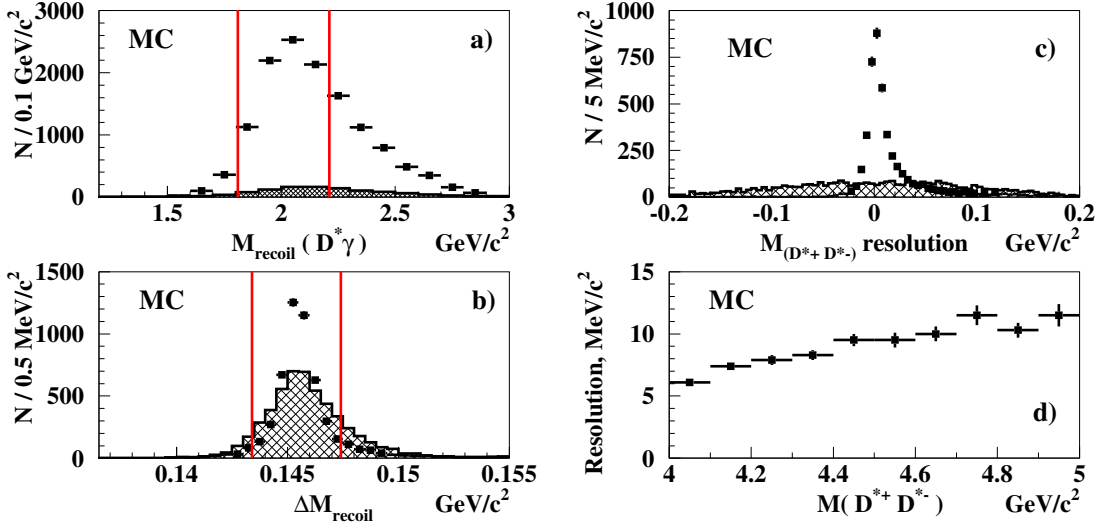


FIG. 1: Monte Carlo distributions for the process  $e^+e^- \rightarrow D^+D^-_{ISR}$ : a)  $M_{recoil}(D^+_{ISR})$  without any requirements on the slow pion (points with error bars), the histogram shows the normalized  $M(D^+)$  sideband contributions; b) the recoil mass difference before (histogram) and after the retting procedure (points with error bars), the selected signal window is shown by the vertical lines; c) the  $M_{recoil}(D^+_{ISR})$  resolution before (histogram) and after the ret procedure (points with error bars); d) the  $M_{D^+D^-}$  resolution as a function of  $M_{D^+D^-}$ .

using Monte Carlo (MC) simulation for  $e^+e^- \rightarrow D^+D^-_{ISR}$ . Similar distributions are obtained for  $e^+e^- \rightarrow D^+D^-_{ISR}$ . The signal MC distribution for  $M_{recoil}(D^+_{ISR})$  is shown in Fig. 1 a). The spread of the peak around the nominal  $D^+$  mass is due to the photon energy resolution; the asymmetric shape is caused by the asymmetric photon resolution function and higher-order corrections to ISR (i.e. more than one ISR in the event). The resolution of this peak,  $\approx 300 \text{ MeV} = c^2$ , is not sufficient to separate  $D^0$ ,  $D^0$  or  $D^0$  final states. To disentangle the contributions from these final states and to suppress combinatorial backgrounds, we use the slow pion from the unreconstructed  $D^+$ . The difference between the mass recoiling against  $D^{(\pm)+}_{ISR}$  and  $D^{(\pm)+}_{slow,ISR}$  (recoil mass difference):

$$M_{recoil} = M_{recoil}(D^{(\pm)+}_{ISR}) - M_{recoil}(D^{(\pm)+}_{slow,ISR}); \quad (2)$$

has a narrow distribution ( $\approx 14 \text{ MeV} = c^2$ ) around the nominal  $M(D^0) - M(D^0)$  mass difference, since the uncertainty in  $D^+$  momentum partially cancels out (Fig. 1 b).

For the measurement of the exclusive cross section, one needs to determine the  $D^{(\pm)+}D^-$  mass when one of the  $D^+$ 's is not reconstructed. In the absence of higher-order QED processes,  $M(D^{(\pm)+}D^-)$  is the mass recoiling against the  $D^+$ . However, the photon energy resolution results in a typical  $M_{recoil}(D^+_{ISR})$  resolution of  $\approx 100 \text{ MeV}$  (Fig. 1 c), which is too wide for the study of relatively narrow  $D^{(\pm)+}D^-$  mass states. We significantly improve the  $M_{recoil}(D^+_{ISR})$  resolution by applying a ret that constrains  $M_{recoil}(D^{(\pm)+}_{ISR})$  to the nominal  $D^+$  mass. In this way we use the well measured properties of the fully reconstructed  $D^{(\pm)+}$  to correct the energy of the  $D^+$ . As a result, the  $M_{D^{(\pm)+}D^-}$  ( $M_{recoil}(D^+_{ISR})$ ) resolution (defined as a width of a core Gaussian in a fit to the resolution function) is improved

by a factor of 10 (see Fig. 1c). Higher-order ISR processes are suppressed by a tight cut on  $M_{\text{recoil}}(D^{(*)+}_{\text{ISR}})$ . The nominal  $M_{D^+D^-}$  resolution, plotted in Fig. 1d), varies from  $6\text{ MeV} = c^2$  around threshold to  $12\text{ MeV} = c^2$  at  $M_{D^+D^-} = 5.0\text{ GeV} = c^2$ . The  $M_{\text{recoil}}$  resolution is also improved by a factor of 2 by the re-fit procedure (Fig. 1b).

Finally, the cross-section is derived from the  $D^{(*)+}D^-$  mass spectrum that is equivalent to the spectrum of recoil mass against the  $D^{(*)+}_{\text{ISR}}$  after the constraint  $M_{\text{recoil}}(D^{(*)+}_{\text{ISR}}) \leq M(D^{(*)+})$ .

## DATA SAMPLE AND SELECTION CRITERIA

The analysis is performed using a data sample collected at the  $(4S)$  resonance and in the nearby continuum with an integrated luminosity corresponding to  $547.8\text{ fb}^{-1}$ .

All charged tracks are required to be consistent with originating from the interaction points (IP) with the requirements:  $dr < 2\text{ cm}$  and  $dz < 4\text{ cm}$ , where  $dr$  and  $dz$  are the impact parameters perpendicular and along the beam direction with respect to the IP. Kaons are required to be positively identified ( $P_K = L_K = (L_K + L_{\bar{K}}) > 0.6$ ) [8]. No identification requirements are applied for pion candidates.

Photons are reconstructed in the electromagnetic calorimeter as showers with energies greater than  $50\text{ MeV}$  that are not associated with charged tracks. At least one energetic photon with energy more than  $2.5\text{ GeV}$  is required in each event. Pairs of photons with energy greater than  $50\text{ MeV}$  are combined to form  $\pi^0$  candidates. If the mass of a pair lies within  $15\text{ MeV} = c^2$  of the nominal  $\pi^0$  mass, the pair is fit with a  $\pi^0$  mass constraint and considered as a  $\pi^0$  candidate.

$K_S^0$  candidates are reconstructed by combining  $\pi^+\pi^-$  pairs with an invariant mass within  $10\text{ MeV} = c^2$  of the nominal  $K_S^0$  mass. The distance between the two pion tracks at the  $K_S^0$  vertex must be less than  $1\text{ cm}$ , the transverse flight distance from the interaction point is required to be greater than  $0.1\text{ cm}$ , and the angle between the  $K_S^0$  momentum direction and decay path in the  $x-y$  plane should be smaller than  $0.1\text{ rad}$ .

$D^0$  candidates are reconstructed using five decay modes:  $K^+\pi^-$ ,  $K^+K^-\pi^+$ ,  $K^+\pi^+\pi^-$ ,  $K_S^0\pi^+$  and  $K^+\pi^0$ . A  $15\text{ MeV} = c^2$  mass window is used for all modes except for  $K^+\pi^+\pi^-$  where a  $10\text{ MeV} = c^2$  requirement is applied ( $\pm 2.5$  in each case).  $D^+$  candidates are reconstructed using decay modes:  $K_S^0\pi^+$ ,  $K^+\pi^+\pi^+$  and  $K^+K^-\pi^+$ . A  $10\text{ MeV} = c^2$  mass window is used for all  $D^+$  modes. To improve their momentum resolution,  $D$  candidates are subjected to a mass-vertex fit constrained to the nominal  $D^0$  or  $D^+$  mass.

$D^-$  candidates are selected via  $D^+\pi^0$  and  $D^0\pi^0$  decay modes with a  $2\text{ MeV} = c^2$  mass-difference window.  $D^0$  reconstruction is required only for background studies. The mass-vertex fit procedure is also applied to  $D^-$  candidates. The DTF procedure allows one to calculate the  $D$  momentum error matrix, which is then used for the fit of  $M_{\text{recoil}}(D_{\text{ISR}})$  to the nominal  $D$  mass.

To suppress contamination from  $e^+e^- \rightarrow D^+D^-$   $_{\text{miss}}^0$   $_{\text{ISR}}$  and higher-order ISR processes, we require  $M_{\text{recoil}}(D^{(*)+}_{\text{ISR}})$  to be within  $0.2\text{ GeV} = c^2$  of the nominal  $D$  mass. We also require the fitted recoil mass difference,  $M_{\text{recoil}}^{\text{fit}}$  to be within  $2\text{ MeV} = c^2$  ( $\pm 2.5$ ) of the nominal  $M(D^{(*)+}) - M(D^0)$  mass difference.

THE STUDY OF THE  $e^+e^- \rightarrow D^+D^-$  EXCLUSIVE CROSS SECTION

The distribution of  $M_{\text{recoil}}(D^+_{\text{ISR}})$  in the data, without any requirements on the slow pion, is shown in Fig. 2a). The excess around the  $D^-$  mass includes the  $e^+e^- \rightarrow D^+D^-$  signal plus overlaps from the  $e^+e^- \rightarrow D^+D^-_{\text{ISR}}$  channel. The shoulder at higher masses is due to  $e^+e^- \rightarrow D^+D^{(*)-}_{\text{ISR}}$ . The excess that is evident at  $\sqrt{s} = 2.5 \text{ GeV} = c^2$  corresponds to  $e^+e^- \rightarrow D^+D^-_{\text{ISR}}$ .

The background from the other processes is substantially suppressed by the inclusion of the slow pion from the unreconstructed  $D^-$  and the tight requirement on  $M_{\text{recoil}}^t$ : i.e. within  $2 \text{ MeV} = c^2$  of the nominal  $M(D^+) - M(D^0)$  mass difference. After the  $M_{\text{recoil}}^t$  requirement, a clean peak corresponding to  $e^+e^- \rightarrow D^+D^-$  is evident in Fig. 2b)

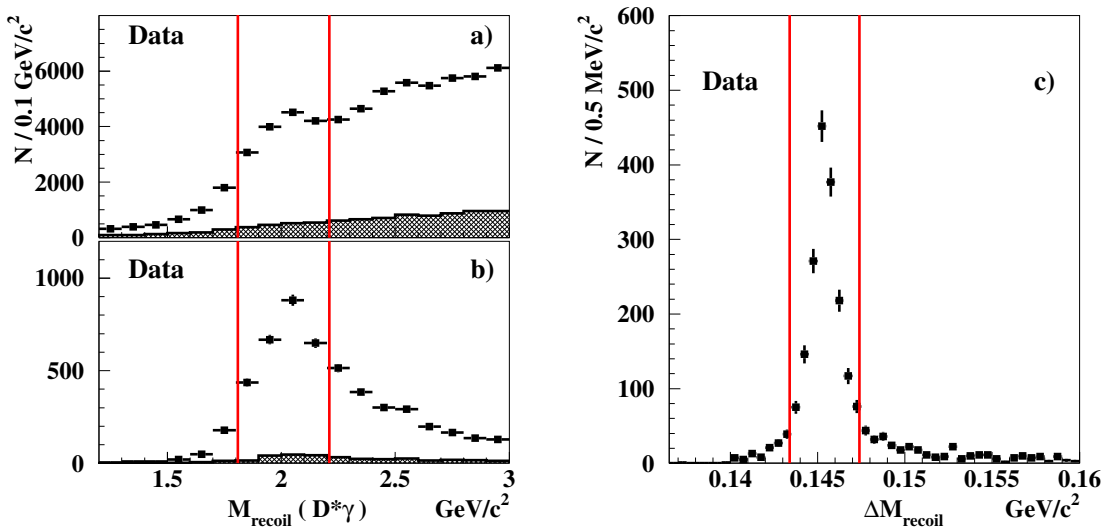


FIG. 2: The  $M_{\text{recoil}}(D^+_{\text{ISR}})$  distributions for the data: a) without requirement of slow pion; b) with  $M_{\text{recoil}}^t$  requirement. Histograms show the normalized  $M(D^+)$  sidebands contributions; the selected signal window is illustrated by vertical lines. c) The distribution of recoil mass difference in the data after the re t procedure. The selected signal window is illustrated by vertical lines.

As mentioned above, we define the signal region by the requirement that  $M_{\text{recoil}}(D^+_{\text{ISR}})$  be within  $0.2 \text{ GeV} = c^2$  of the nominal  $D^-$  mass. This requirement is needed to suppress  $e^+e^- \rightarrow D^+D^0_{\text{ISR}}$  events, which have a similar  $M_{\text{recoil}}^t$  distribution. The spectrum of recoil mass differences for the signal  $M_{\text{recoil}}(D^+_{\text{ISR}})$  window after the  $M_{\text{recoil}}^t$  re t procedure in data is shown in Fig. 2c).

Multiple candidates

Approximately 8% of the finally selected events have multiple entries (including those events where both the  $D^+$  and  $D^-$  are fully reconstructed and, thus, automatically counted twice). In these cases, the  $D^+$  candidate with the minimum value of  $\chi^2_{\text{tot}}$ :

$$\chi^2_{\text{tot}} = \chi^2_{M(D^0)} + \chi^2_{M(D^+)} + \chi^2_{M_{\text{recoil}}^t}; \quad (3)$$

is chosen, where each  $\sigma^2$  is defined as the squared ratio of the deviation of the measured parameter from the expected signal value and the corresponding resolution.

For multiple-entry events in our background studies, where we select candidates from the  $M(D^+)$  and  $M_{recoil}^t$  sidebands, we apply a similar single candidate selection procedure for the sideband regions, in which case  $\sigma_{M(D^+)}^2$  and  $\sigma_{M_{recoil}^t}^2$  are calculated with respect to the center of the corresponding sideband.

## Backgrounds

The following sources of background are considered:

- (1) combinatorial background under the reconstructed  $D^+$  peak;
- (2) real  $D^+$  mesons coming from the signal or other processes combined with a combinatorial slow pion;
- (3) both the  $D^+$  and slow pion are combinatorial;
- (4) reflection from the process  $e^+e^- \rightarrow D^+D^0_{miss}ISR$  with an extra  $D^0$  in the final state;
- (5) contribution of  $e^+e^- \rightarrow D^+D^0$  when an energetic  $D^0$  is misidentified as a single

$ISR$ .

The contributions of backgrounds (1) and (2) are extracted using  $D^+$  ( $2.012 \text{ GeV} = c^2 < M(D^+) < 2.020 \text{ GeV} = c^2$ ) and  $M_{recoil}^t$  ( $0.010 \text{ GeV} = c^2 < (M_{recoil}^t - 0.1454) < 0.018 \text{ GeV} = c^2$ ), which have twice the area of the signal region. The latter sideband is shifted from the signal region to avoid signal over-subtraction due to the higher-order ISR tail. Background (3) is present in both the  $M(D^+)$  and  $M_{recoil}^t$  sidebands and is, thus, subtracted twice. To account for this over-subtraction we use a double sideband region, when events are selected from both the  $D^+$  and the  $M_{recoil}^t$  sidebands.

Finally, the background contributions (1-3) are estimated as:

$$M(D^+D^0)_{Bkg(1-3)} = \frac{1}{2} M(D^+D^0)_{sbD} + \frac{1}{2} M(D^+D^0)_{sb} - \frac{1}{4} M(D^+D^0)_{sbD} \quad (4)$$

where the factors account for the different areas of the selected signal and sideband regions. Uncertainties in these factors due to possible non-uniform background distribution are included in the systematic error. The total contribution from combinatorial backgrounds (1-3) is shown in Fig. 3 a) and is subtracted from the signal-region  $D^+D^0$  mass spectrum.

Process (4) produces a broad peak in the  $M_{recoil}^t$  distribution around the nominal  $M(D^+) - M(D^0)$  mass difference and, thus, is not contained in the  $M_{recoil}^t$  sidebands. The dominant part of this background is suppressed by the tight requirement on  $M_{recoil}(D^+ISR)$ . The remaining part is estimated by applying a similar partial reconstruction method to the isospin conjugate final state: a  $D^0$  is fully reconstructed and the slow pion from a  $D^+$  is used for the recoil mass difference requirement. Since there is a charge imbalance in this final state, only events with a missing extra  $D^+$  can contribute to the recoil mass difference peak. To extract the level of background (4), this spectrum is rescaled according to the ratio of  $D^0$  and  $D^+$  reconstruction efficiencies and a factor of 1/2 due to isospin statistics:

$$\epsilon_{ref} = 1/2 \cdot \epsilon_{D^+} = \epsilon_{D^0} \quad (5)$$

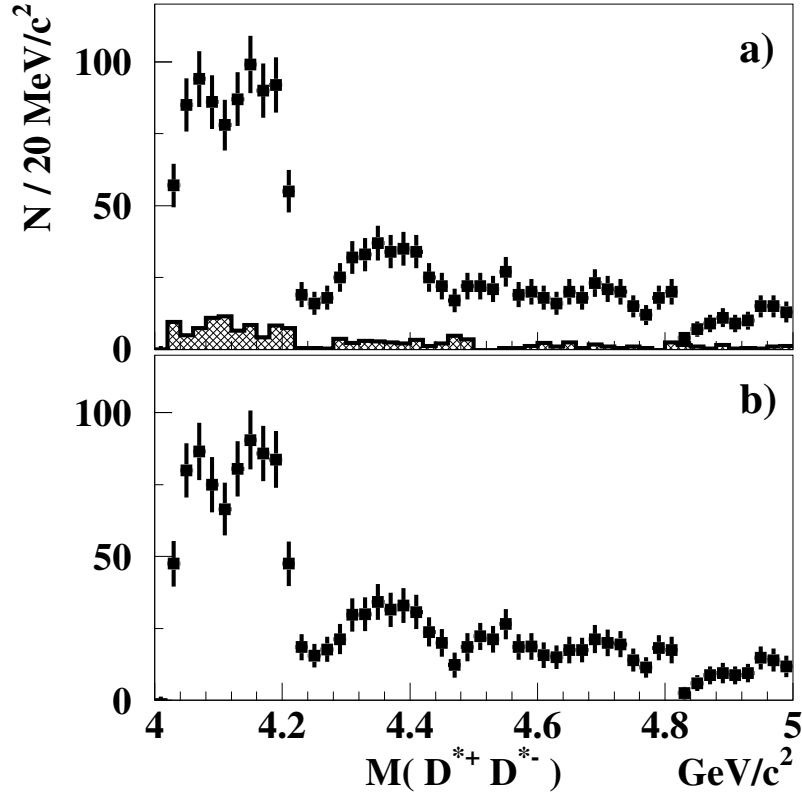


FIG. 3: The  $D^+D^-$  mass distribution for the data: a) for the signal box events (points with error bars), total combinatorial background (1-3) shown as hatched histogram; b) after background subtraction.

The contribution from background (4) is found to be consistent with zero. Uncertainties in this estimate are included in the systematic error.

The contribution of background (5), where an energetic  $\pi^0$  is misidentified as a  $\pi_{ISR}^0$  is determined from the data using reconstructed  $e^+e^- \rightarrow D^+D^-\pi^0$  events using a similar partial reconstruction technique but with an energetic  $\pi^0$  replacing the  $\pi_{ISR}^0$ . The contribution of this background is found to be negligibly small; uncertainties in this estimate are included in the systematic error.

The background-subtracted  $D^+D^-$  mass distribution is shown in Fig. 3 b).

#### THE STUDY OF THE $e^+e^- \rightarrow D^+D^-$ EXCLUSIVE CROSS SECTION

The analysis of the  $e^+e^- \rightarrow D^+D^-$  exclusive cross section with initial state radiation (ISR) is identical to that described above for  $e^+e^- \rightarrow D^+D^-$  with the fully reconstructed  $D^+$  meson replaced by a fully reconstructed  $D^+$  meson. The distribution of  $M_{\text{recoil}}(D^+_{ISR})$  with no requirements on the slow pion from the  $D^-$  is presented in Fig. 4 a). The excess around the nominal  $D^-$  mass corresponds to the  $e^+e^- \rightarrow D^+D^-$  signal plus overlaps from the  $e^+e^- \rightarrow D^+D^-_{ISR}$  channel. The shoulder at higher masses is due to  $e^+e^- \rightarrow D^{(*)+}D^-_{ISR}$ .

The requirement of a detected slow pion from the unreconstructed  $D^+$  and a tight requirement on  $M_{\text{recoil}}^{\text{t}}$  provides the clean  $e^+e^- \rightarrow D^+D^0$  signal peak that is shown in Fig. 4 b). The recoil mass difference distribution for the signal  $M_{\text{recoil}}(D^+ \text{ ISR})$  window, after the  $M_{\text{recoil}}^{\text{t}}$  re t procedure, is shown in Fig. 4 c).

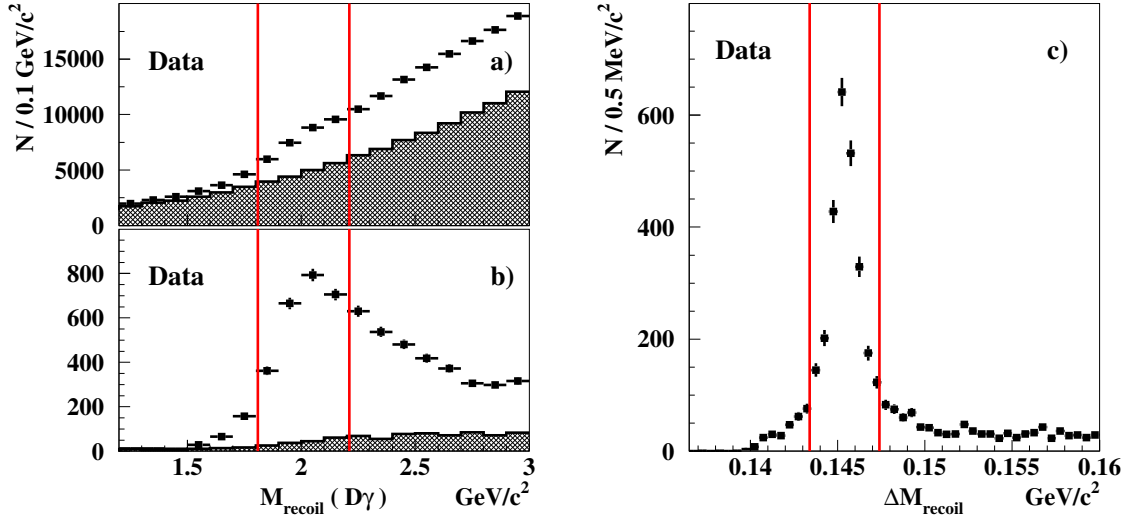


FIG. 4: Data. The  $M_{\text{recoil}}(D^+ \text{ ISR})$  distribution: a) without a requirement on the slow pion; b) with a  $M_{\text{recoil}}^{\text{t}}$  requirement. Histograms show the normalized  $M(D^+)$  sidebands contributions. c) The distribution of recoil mass difference after the re t procedure. The selected signal window is indicated by the vertical lines.

#### Multiple counting candidates

In the case of multiple entries, we apply a single candidate selection procedure similar to that used for  $D^+D^0$  to all the distributions shown below.

#### Backgrounds

The following sources of background are considered:

- (1) combinatorial background under the reconstructed  $D^+$  peak;
- (2) real  $D^+$  mesons coming from the signal or other processes combined with a combinatorial slow pion;
- (3) both the  $D^+$  and slow pion are combinatorial;
- (4) reflection from the process  $e^+e^- \rightarrow D^+D^0_{\text{miss}} \text{ ISR}$  with an extra  $0$  in the final state;
- (5) reflection from the process  $e^+e^- \rightarrow D^+D^0_{\text{ISR}}$  followed by  $D^+ \rightarrow D^0_{\text{miss}}$  with missed  $0$ ;

(6) contribution of  $e^+e^- \rightarrow D^+D^0$  when the energetic  $D^0$  is misidentified as a single

ISR.

The contributions of backgrounds (1-3) are determined using  $D^+$  ( $0.03 < M(D^+) < 1.869$  GeV) and  $M_{\text{recoil}}^t$  ( $0.010 \text{ GeV} = c^2 < (M_{\text{recoil}}^t - 0.1454) < 0.018 \text{ GeV} = c^2$ ) sidebands with twice the area of the signal region. Here again, background (3) is present in both  $M(D^+)$  and  $(M_{\text{recoil}}^t - 0.1454)$  sidebands and thus subtracted twice. To account for this over-subtraction we use a double sideband region which consists of pure background (3) events. Finally background (1-3) contribution are estimated as:

$$M(D^+D^0)_{\text{Bkg(1-3)}} = \frac{1}{2} M(D^+D^0)_{\text{sbD}} + \frac{1}{2} M(D^+D^0)_{\text{sb}} - \frac{1}{4} M(D^+D^0)_{\text{sbD}} \quad (6)$$

The total combinatorial background (1-3) is shown as the hatched histogram in Fig. 5 a). The  $D^+D^0$  mass distribution after combinatorial backgrounds subtraction is shown in Fig. 6.

The level of contamination from backgrounds (4-5) is determined from isospin conjugate events,  $e^+e^- \rightarrow D^0D^+$  in the data. The  $D^+D^0$  analysis is repeated with the fully reconstructed  $D^+$ 's replaced by fully reconstructed  $D^0$ 's. To calculate the ratio of the efficiencies for two isospin conjugate modes we use Monte Carlo simulations of  $e^+e^- \rightarrow D^+D^0$  followed by  $D^+ \rightarrow D^0\pi^+$  and  $e^+e^- \rightarrow D^+D^0$  followed by  $D^+ \rightarrow D^+\pi^0$  processes.

The combinatorial background subtraction procedure for process (4-5) is similar to that described for the  $D^+D^0$  process. The obtained  $D^0D^+$  mass distribution for events in the signal region is presented in Fig. 5 b).

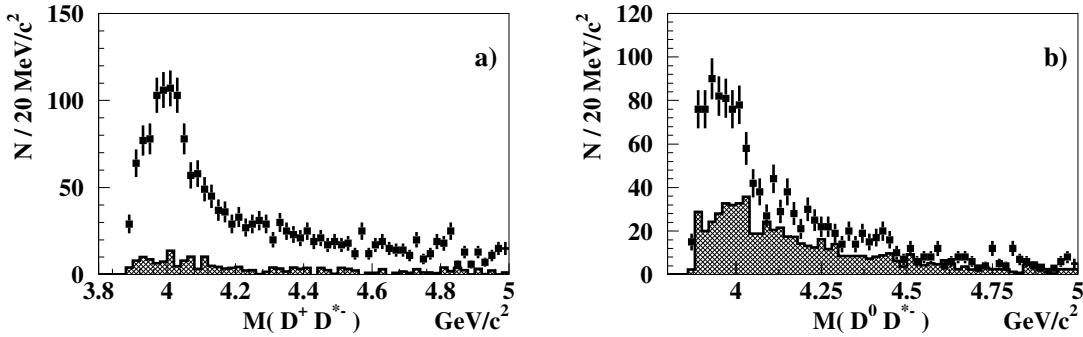


FIG. 5: a) The  $D^+D^0$  mass distribution for the signal region (points with error bars). The total combinatorial background (1-3) is shown as the hatched histogram. b) The  $D^0D^+$  mass distribution for the signal region (points with errors bars). The total combinatorial background is shown as the hatched histogram.

To calculate the contribution of background (4-5), the  $D^0D^+$  mass distribution, after combinatorial background subtraction, is rescaled according to the ratio of  $D^+$  and  $D^0$  reconstruction efficiencies and by the  $D^+$ ,  $D^+$ ,  $D^0$  branching fractions that are not included in the MC simulation. The combined background (4) and (5) contribution is indicated in Fig. 6 by the triangular data points.

The contribution from background (6), where an energetic  $D^0$  is misidentified as a ISR, is determined from reconstructed  $e^+e^- \rightarrow D^+D^0$  events in the data. This is found to be negligibly small and taken into account in the systematic error.

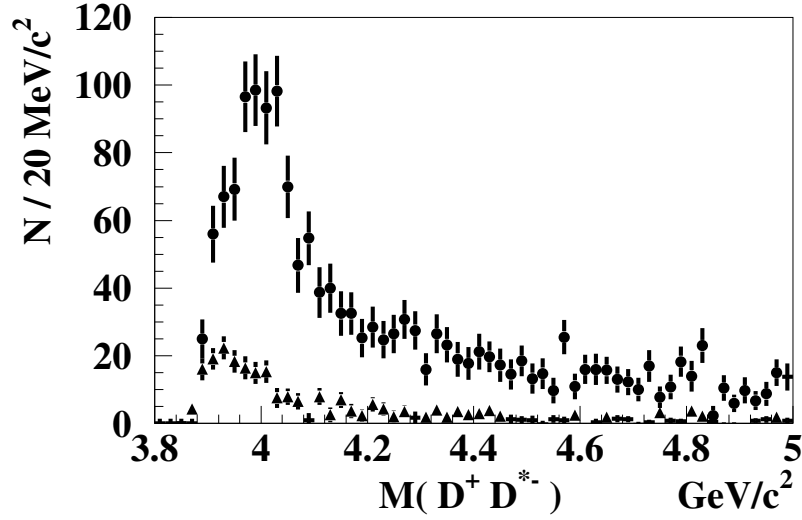


FIG. 6:  $D^+D^{*0}$  mass spectra for the studied process after combinatorial backgrounds (1-3) subtraction (points with error bars). Contribution of (4-5) process (triangles with error bars).

#### CROSS-SECTION CALCULATION

The  $e^+e^- \rightarrow D^{(*)+}D^{*0}$  cross sections are extracted from the  $D^{(*)+}D^{*0}$  mass distributions by the relation [10]:

$$\sigma_{e^+e^- \rightarrow D^{(*)+}D^{*0}} = \frac{dN/dm}{\text{tot} dL/dm}; \quad (7)$$

where  $m = M(D^{(*)+}D^{*0})$ ,  $dN/dm$  is the mass spectra obtained before corrections for resolution and higher-order radiation,  $dL/dm$  is the differential ISR luminosity and  $\text{tot}$  is the total efficiency. The differential luminosity  $dL/dm$  is:

$$dL/dm = \frac{1}{x} (2 - 2x + x^2) \ln \frac{1+C}{1-C} - x^2 C \frac{2mL}{E_{CM}^2}; \quad (8)$$

where  $x = 1 - m^2/E_{CM}^2$ ,  $E_{CM}$  is the nominal  $e^+e^-$  CM energy,  $L$  is the total integrated luminosity and  $C = \cos \theta_0$ , where  $\theta_0$  defines the polar angle range for  $\text{ISR}$  in the  $e^+e^-$  CM frame:  $0 < \theta_{\text{ISR}} < 180 - \theta_0$ .

The reconstruction efficiencies, determined as a function of by MC simulation, are found to be independent of  $M(D^{(*)+}D^{*0})$  for both processes being studied, and are equal to  $\langle \epsilon(D^+D^0) \rangle = 4.28 \cdot 10^{-3}$  and  $\langle \epsilon(D^+D^{*0}) \rangle = 3.87 \cdot 10^{-3}$ , respectively.

The resulting exclusive  $e^+e^- \rightarrow D^{(*)+}D^{*0}$  cross-sections are shown in Fig. 7. Since the bin width is much larger than the resolution, the distributions are not corrected for resolution.

#### SYSTEMATIC ERRORS

The systematic errors for the  $(e^+e^- \rightarrow D^{(*)+}D^{*0})$  measurements are summarized in Table I. To determine the systematic errors associated with the background subtraction, we

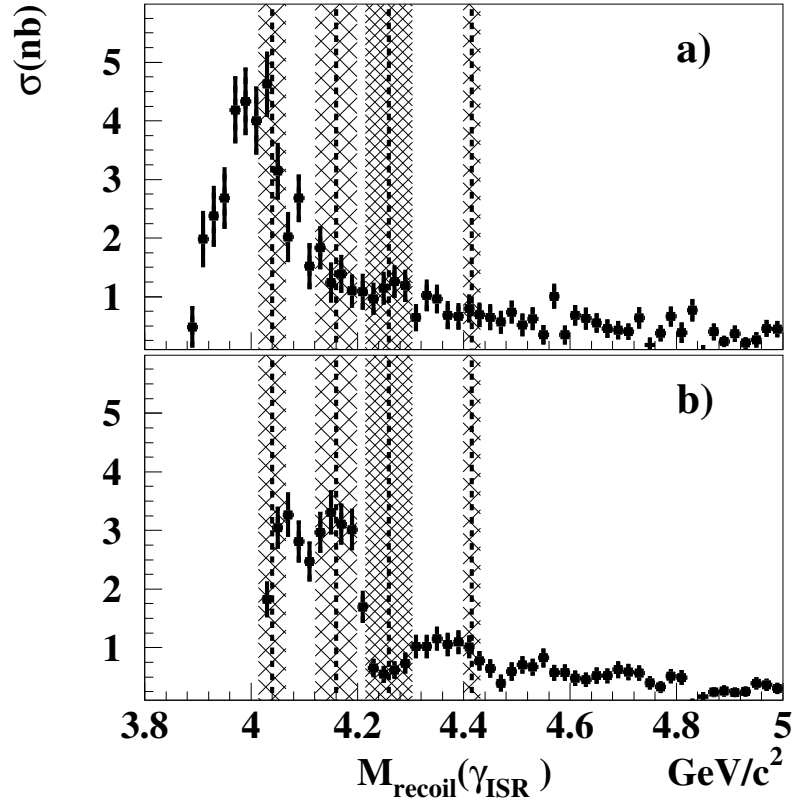


FIG .7: The exclusive cross-sections for a)  $e^+e^- \rightarrow D^+D^-$  and b)  $e^+e^- \rightarrow D^+D^0$ . The dashed lines correspond to the  $(4040)$ ,  $(4160)$  and  $(4415)$  masses; the widths of hatched areas are equal to their respective full widths [9]. The dashed line and the width of densely hatched area corresponds to the mass and full width of the  $Y(4260)$  resonance reported by BaBar [5].

estimate the uncertainty in the scaling factors for the sideband subtractions (Eqn.(4,6)) using fits to  $M(D^{(*)+})$  and  $M_{\text{recoil}}^+$  distributions in the data with different signal and background parameterizations. The scaling factor extracted from the integral under the background function for the signal and sideband regions varies by less than 20% for both  $D^+D^-$  and  $D^+D^0$ . Since the total combinatorial backgrounds (1-3) are only 15% of the signal, the net uncertainty is 3%. Uncertainties in backgrounds (4-5) are estimated conservatively to be smaller than 2% of the signal in the case of  $D^+D^-$ ; these two sources are added linearly to give 5% in total. In the case of the  $D^+D^0$ , backgrounds (4-5) are subtracted using the data and only the uncertainty in the scaling factor for the subtracted distribution is taken into account.

A second source of systematic error is due to the unknown helicity-angle distributions in the  $D^+D^-$  final state. These final states can be mixtures of  $D_T^+D_T^-$ ,  $D_T^+D_L^-$  and  $D_L^+D_L^-$ , where the subscripts L and T stand for longitudinally and transversely polarized  $D^{\pm}$ 's. For the efficiency calculation, we assume equal fractions of these helicity states, and consider the extreme cases (pure  $D_T^+D_T^-$  and pure  $D_L^+D_L^-$ ) for the efficiency uncertainty. There is no corresponding uncertainty in case of  $D^+D^0$  final state, where the  $D^0$  polarization is fixed by angular momentum and parity conservation.

TABLE I: Contributions to the systematic error on the cross sections, [%].

Source	Systematic error (%)	
	$D^+D^-$	$D^+D^0$
Background subtraction	5	4
Angular distributions	5	1
Reconstruction	7	6
Cross section calculation	2	2
$B(D^{\prime})$	3	5
MC statistics	2	1
Identification	1	1
Total	11	9

A third source of systematic error comes from the uncertainties in track and photon reconstruction efficiencies, which are 1% per track, 2% per slow pion and 1.5% per photon, respectively.

The systematic error ascribed to the cross section calculation is estimated by the study of the  $\sqrt{s}$ -dependence of the final result and includes a 1.5% error on the total luminosity. Other contributions come from the uncertainty in the kaon identification efficiency and the absolute  $D^0$  and  $D^{\prime+}$  branching fractions.

The total systematic uncertainties are approximately the same as the statistical errors in the peaks of the differential cross-sections.

## SUMMARY

In summary, we report first measurements of exclusive  $e^+e^- \rightarrow D^+D^-$  and  $e^+e^- \rightarrow D^+D^0$  cross sections at  $\sqrt{s}$  around the  $D^+D^-$  and  $D^+D^0$  thresholds with initial state radiation. The shapes of the cross section distributions are similar to that of the inclusive  $e^+e^-$  hadronic cross section measured by BES and Crystal Ball. The values of the cross sections obtained are compatible within errors with the  $D^{\prime} \bar{D}^{\prime}$  exclusive cross section in the energy region up to 4260 GeV measured by CLEO-c. The local minimum in the exclusive  $e^+e^- \rightarrow D^+D^-$  cross section is surprisingly close both to the  $Y(4260)$  mass and to the  $D_s^+D_s^-$  threshold [1]. Analyses of the  $D^+D^-$  and  $D^0\bar{D}^0$  final states are in progress.

## ACKNOWLEDGMENTS

We thank the KEKB group for the excellent operation of the accelerator, the KEK cryogenics group for the efficient operation of the solenoid, and the KEK computer group and the National Institute of Informatics for valuable computing and Super-SINET network support. We acknowledge support from the Ministry of Education, Culture, Sports, Science, and Technology of Japan and the Japan Society for the Promotion of Science; the Australian Research Council and the Australian Department of Education, Science and Training; the National Science Foundation of China and the Knowledge Innovation Program of the Chinese Academy of Sciences under contract No. 10575109 and IHEP-U-503; the Department

of Science and Technology of India; the BK 21 program of the Ministry of Education of Korea, and the CHEP SRC program and Basic Research program (grant No. R01-2005-000-10089-0) of the Korea Science and Engineering Foundation; the Polish State Committee for Scientific Research under contract No. 2P 03B 01324; the Ministry of Science and Technology of the Russian Federation; the Slovenian Research Agency; the Swiss National Science Foundation; the National Science Council and the Ministry of Education of Taiwan; and the U.S. Department of Energy.

- 
- [1] J.Z. Bai, et al. (BES Collab.), *PhysRevLett.*, 88, 101802 (2002), [[hep-ex/0102003](#)].
  - [2] A. Osterheld et al. SLAC-PUB-4160, Dec 1986. 57pp.
  - [3] R. Poling, "CLEO-C Hot Topics", [hep-ex/0606016](#), FCCP2006 (Vancouver 2006)
  - [4] T.E. Coan, et al. (CLEO Collab.), *PhysRevLett.*, 96, 162003 (2006), [[hep-ex/0602034](#)].
  - [5] B. Aubert, et al. (BABAR Collab.), *PhysRevLett.*, 95, 142001 (2005), [[hep-ex/0506081](#)].
  - [6] charge conjugation is implied throughout this paper
  - [7] B. Aubert, et al. (BABAR Collab.), *PhysRev.*, D 70, 072004 (2004), [[hep-ex/0408078](#)].
  - [8] E Nakano, *NuclInstrum Meth.*, A 494 402 (2002).
  - [9] S. Eidelman et al. (Particle Data Group), *Phys. Lett. B* 592, 1 (2004) and (2005) update at <http://pdg.lbl.gov>.
  - [10] B. Aubert, et al. (BABAR Collab.), *PhysRev.*, D 73, 012005 (2006), [[hep-ex/0512023](#)].
  - [11] M.B. Voloshin, "Channel coupling in  $e^+e^-$  annihilation into heavy meson pairs at the  $D^* \text{ anti-}D^* \text{ threshold}$ ", [hep-ph/0602233](#).